

## Free energy sources in current sheets formed in collisionless plasma turbulence

NEERAJ JAIN,<sup>1</sup> JÖRG BÜCHNER,<sup>1</sup> HORIA COMIŞEL,<sup>2</sup> AND UWE MOTSCHMANN<sup>3</sup>

<sup>1</sup>*Zentrum für Astronomie und Astrophysik, Technische Universität Berlin, Hardenbergstr. 36, D-10623, Berlin, Germany*

<sup>2</sup>*Institute for Space Sciences, P.O. Box MG-23, Atomistilor 409, 077125 Bucharest-Magurele, Romania*

<sup>3</sup>*Institut für Theoretische Physik, Technischen Universität Braunschweig Mendelssohnstr. 3, D-38106 Braunschweig, Germany*

### ABSTRACT

An unsolved problem of the usually collisionless and turbulent space plasmas, e.g., of the solar wind or the magnetosheath of the Earth's magnetosphere, is the mechanism of dissipation of macroscopic energy into heat without collisional viscosity and electrical resistivity. The most viable process under consideration is the turbulent cascade of energy from macroscopic to kinetic scales, where collisionless plasma processes finally dissipate the energy into heat. Meanwhile space observations and numerical simulations have shown that in such turbulent plasmas current sheets form at kinetic scales. Instabilities in these current sheets can provide collisionless dissipation and influence the properties of the turbulence. Spatial gradients of the macroscopic physical parameters and non-Maxwellian features of the velocity space distribution functions provide the sources of free energy for current sheet plasma instabilities. In order to determine the free energy sources provided by the spatial gradients of plasma number density and electron/ion bulk velocities in current sheets formed in collisionless turbulent plasmas with

an applied external magnetic field, we carried out two-dimensional PIC-hybrid-code simulations.

We found that current sheets in a collisionless turbulent plasma are formed primarily by electron shear flows with electron bulk velocity much larger than the ion bulk velocity while the density variations through the current sheets are relatively small ( $< 10\%$ ). The electron bulk velocities and, thus, the current densities inside the sheets are directed mainly parallel to the external magnetic field. The shear in the perpendicular electron and ion bulk velocities generates electron- and ion-flow vorticities in the direction parallel to the external magnetic field. Inside the current sheets the parallel electron-flow vorticity exceeds the parallel ion-flow vorticity, it changes its sign around the current sheet centers and peaks near the edges of current sheets. An ion temperature anisotropy develops near current sheets during their formation. It correlates well with the parallel ion vorticity as well as with the parallel electron vorticity. Theoretical estimates in the limit of un-magnetized ions support the simulation results.

*Keywords:* Current sheets, kinetic plasma turbulence, hybrid simulations, free energy sources

## 1. INTRODUCTION

In collisionless plasmas ranging from hot laboratory to dilute astrophysical plasmas, irreversible dissipation of macroscopic energy into heat, without the normal channels of viscosity and electrical resistivity, is a key unsolved problem. Turbulent transfer of the energy from macroscopic to micro scales (kinetic scales such as Larmor radii and inertial lengths of plasma particles), where it is finally dissipated into heat by kinetic plasma processes, is considered one of the most viable mechanism of the dissipation in collisionless plasmas (Marsch 2006). The energy transfer from macroscopic to kinetic scales takes place by an anisotropic cascade process mediated by Alfvén waves (Howes 2015; Loureiro & Boldyrev 2017). At kinetic scales, plasma processes dissipate the energy by first transferring it from turbulent electromagnetic fields to plasma particles by field-particle interactions. The resulting

velocity space structures are then supposed to be driven by an entropy cascade to scales small enough that even the infrequent collisions can thermalize the particles (Schekochihin et al. 2009).

At kinetic scales, both the homogeneously distributed (Hollweg & Isenberg 2002; Leamon et al. 1998; Bale et al. 2005; Schekochihin et al. 2009; Howes et al. 2011; Podesta 2012; Gary et al. 2016; Chandran et al. 2010; Bourouaine & Chandran 2013) and inhomogeneous localized (Dmitruk et al. 2004; Sundkvist et al. 2007; Parashar & Matthaeus 2016; Chasapis et al. 2017; Karimabadi et al. 2013; Wan et al. 2015; Osman et al. 2011, 2014) plasma processes dissipate the turbulence energy. An increasing number of observational and simulation studies in recent years support the inhomogeneous intermittent dissipation localized in and around kinetic scale current sheets which form self consistently in plasma turbulence and contain significant power of the turbulence (Matthaeus et al. 2015; Borovsky 2010). Current sheets with thicknesses ranging from ion to electron scales are observed ubiquitously in numerical simulations and space observations of collisionless plasma turbulence (Sundkvist et al. 2007; Biskamp & Welter 1989; Maron & Goldreich 2001; Franci et al. 2015; Perri et al. 2012; Howes 2016; Podesta 2017). Therefore, an understanding of kinetic plasma processes in current sheets formed in kinetic plasma turbulence is crucial to solve the puzzle of dissipation and heating in turbulent collisionless plasmas, e.g., the solar wind, solar corona and Earth's magnetosphere.

Several kinetic plasma processes, mainly, stochastic ion heating (Markovskii & Vasquez 2011), Landau and cyclotron damping (TenBarge & Howes 2013), and acceleration by parallel electric fields (Egedal et al. 2012) and Fermi acceleration in contracting magnetic islands (Drake et al. 2006) generated by magnetic reconnection, have been proposed as collisionless mechanisms of the energy dissipation in current sheets. These kinetic plasma processes are either the direct consequences of or influenced by plasma instabilities which can grow in kinetic scale current sheets. Tearing instability in current sheets causes magnetic reconnection which can energize plasma particles by parallel electric fields and/or by Fermi acceleration in contracting magnetic islands generated in the process (Ergun et al. 2017; Muñoz & Büchner 2017). Tearing instability of an ion-scale current sheet can be enhanced by ion cyclotron instability while suppressed by firehose instability (Gingell et al.

2015). Plasma instabilities in current sheets can generate large amplitude plasma waves which can lead to the stochastic ion heating (Demchenko & Hussein 1974).

Plasma instabilities in current sheets have also been suggested to influence the location of the ion scale break observed in the power spectrum of plasma turbulence. Laboratory experiments of magnetic reconnection strongly suggest a connection between the ion-scale spectral break, observed near lower hybrid frequency in the experiments, and instabilities of a single current sheet (von Stechow et al. 2016). In solar wind turbulence, the location (near ion cyclotron frequency) of the ion-scale break was linked to the current sheet thickness which is a crucial parameter to determine the growth of the plasma instabilities in current sheets (Borovsky & Podesta 2015). It was also observed to depend on the amplitude of the magnetic field fluctuations (Markovskii et al. 2008) which can be controlled by plasma instabilities in current sheets.

Numerical simulations, space observations, laboratory experiments and theoretical studies of collisionless plasma turbulence and individual current sheets, therefore, suggest that plasma instabilities in current sheets formed in plasma turbulence can play an important role not only in collisionless dissipation but also in the kinetic scale properties of the observed turbulence spectra, in particular the spectral breaks. Growth of plasma instabilities depends on free energy sources available from spatial gradients of physical quantities and/or from non-Maxwellian features of plasma particles' distribution functions. A clear understanding of the free energy sources available in the current sheets formed in collisionless plasma turbulence is, therefore, essential to pin point the role of plasma instabilities in the turbulence.

In a current sheet, current density  $\mathbf{J} = ne(\mathbf{u}_i - \mathbf{u}_e)$  ( $n$  and  $\mathbf{u}_{i,e}$  are plasma number density and ion/electron bulk velocities, respectively) is confined in a small thickness. Therefore, free energy sources in a current sheet can come from spatial gradients of  $n$ ,  $\mathbf{u}_i$  and  $\mathbf{u}_e$ . In addition, the non-Maxwellian features in the forms of temperature anisotropy and/or relative drift of plasma particles might also be present. Ion temperature anisotropy is often observed near the current sheets formed in collisionless plasma turbulence. Relative contributions of  $n$ ,  $\mathbf{u}_i$  and  $\mathbf{u}_e$  in the formation of the current sheets in the turbulence are, however, not known yet.

In this paper, we carry out 2-D PIC-hybrid simulations of collisionless plasma turbulence to study the relative contributions of  $n$ ,  $\mathbf{u}_i$  and  $\mathbf{u}_e$  in the formation of the current sheets in the turbulence. We find that current sheets are formed primarily by electron shear flow, i.e., electron bulk velocity is much larger than ion bulk velocity and density variation is relatively small ( $< 10\%$ ) inside current sheets. Electron bulk velocity and thus current inside sheets are directed mainly parallel to the external magnetic field. Shear flow in perpendicular bulk velocities of electrons and ions generates parallel components of electrons and ions vorticity, the former of which is larger than the later inside current sheets, changes sign around the center and peaks near the edges of current sheets. Ion temperature anisotropy develops near current sheets during the formation of current sheets and correlates well with both the electron and ion vorticities. Theoretical estimates in the limit of un-magnetized ions support the simulation results.

The paper is organized as follows. Section 2 describes the simulation setup. Results are presented in section 3. Theoretical estimates are presented in section 4. Discussion of results and conclusion are presented in section 5.

## 2. SIMULATION SETUP

We employ a hybrid model of plasmas in which ions are treated as particles while electrons as an inertia-less fluid. Such plasma model leaves out electron inertial and electron kinetic effects important at electron scales. Our 2-D simulations are carried out using a PIC-hybrid code A.I.K.E.F. of the Technical University Braunschweig (Müller et al. 2011). We initialize our 2-D simulations in an x-y plane with random phased fluctuations of magnetic field and plasma velocity imposed on a isotropic background plasma of uniform density  $n_0$ . A uniform magnetic field  $B_0\hat{z}$  is applied perpendicular to the simulation plane. Magnetic field fluctuations are calculated from magnetic vector potential

$$\tilde{\mathbf{A}} = \hat{z} \sum_{k_x, k_y} \delta A_z(k_x, k_y) \sin(k_x x + k_y y + \phi(k_x, k_y)), \quad (1)$$

where  $k_x$  and  $k_y$  are wave numbers in x- and y-direction, respectively, and  $\phi$  is the wave-number dependent random phase. The amplitude  $\delta A_z$  of the magnetic vector potential is so chosen that the amplitude of magnetic field fluctuation  $\delta B_\perp = \delta A_z k_\perp$  is independent of the wave number, i.e.,

all initialized modes have the same energy. Plasma velocity fluctuations have the same form as magnetic field fluctuations except the random phases so that the magnetic and velocity fluctuations have vanishing correlation but equi-partition of energy.

We initialize fluctuations in the wave number range  $|k_{x,y}d_i| < 0.2$  ( $k_{x,y} \neq 0$ ) to have a root-mean-square value  $B_{rms}/B_0 = 0.24$ . Here  $d_i = v_{Ai}/\omega_{ci}$ ,  $v_{Ai} = B_0/\sqrt{\mu_0 n_0 m_i}$  and  $\omega_{ci} = eB_0/m_i$  are inertial length, Alfvén velocity and cyclotron frequency of ions, respectively, and,  $\mu_0$  (vacuum magnetic permeability),  $e$  (electronic charge) and  $m_i$  (proton mass) are physical constants. Electron and ion plasma beta are  $\beta_e = 2\mu_0 n_0 k_B T_e / B_0^2 = 0.5$  and  $\beta_i = 2\mu_0 n_0 k_B T_i / B_0^2 = 0.5$ , respectively. Here  $T_e$  and  $T_i$  are electron and ion temperatures, respectively, and  $k_B$  is the Boltzmann constant. The simulation box size  $256d_i \times 256d_i$  is fixed for  $512 \times 512$ ,  $1024 \times 1024$  and  $2048 \times 2048$  grid points with 500, 1000 and 2000 particles per cell, respectively. The time step for the three grid sizes are  $\Delta t = 0.01$ , 0.0025 and  $0.001 \omega_{ci}^{-1}$ , respectively. Such small values of time step allows us to take collisional resistivity as zero in all simulations. Boundary conditions are periodic in all directions.

### 3. SIMULATION RESULTS

The random-phased fluctuations of magnetic field and ion bulk velocity initialized at long wavelength in our simulations evolve to form current sheets. Evolutions of root-mean-square (RMS) values of perpendicular magnetic field  $\mathbf{B}_\perp$  and parallel current density  $J_z$  are shown in Fig. 1, where RMS value of a variable  $\psi$  is calculated as

$$\psi^{rms} = [\langle \psi^2 \rangle - \langle \psi \rangle^2]^{1/2}. \quad (2)$$

Here parallel and perpendicular directions are with respect to the (z-) direction of the applied magnetic field. RMS values grow from their initial values to reach maximum values and then decay slowly. The time of reaching maximum for  $B_\perp^{rms}$ ,  $\omega_{ci}t = 50$ , is different from that for  $J_z^{rms}$  (at  $\omega_{ci}t = 150$ ). Fig. 2 shows parallel current density  $J_z$  in the whole simulation domain at the two times when  $B_\perp^{rms}$  and  $J_z^{rms}$  reach maximum. Current sheets get formed in the turbulence by  $\omega_{ci}t = 50$ . A typical current sheet at  $\omega_{ci}t = 50$  has a central current accompanied by return side currents (opposite to

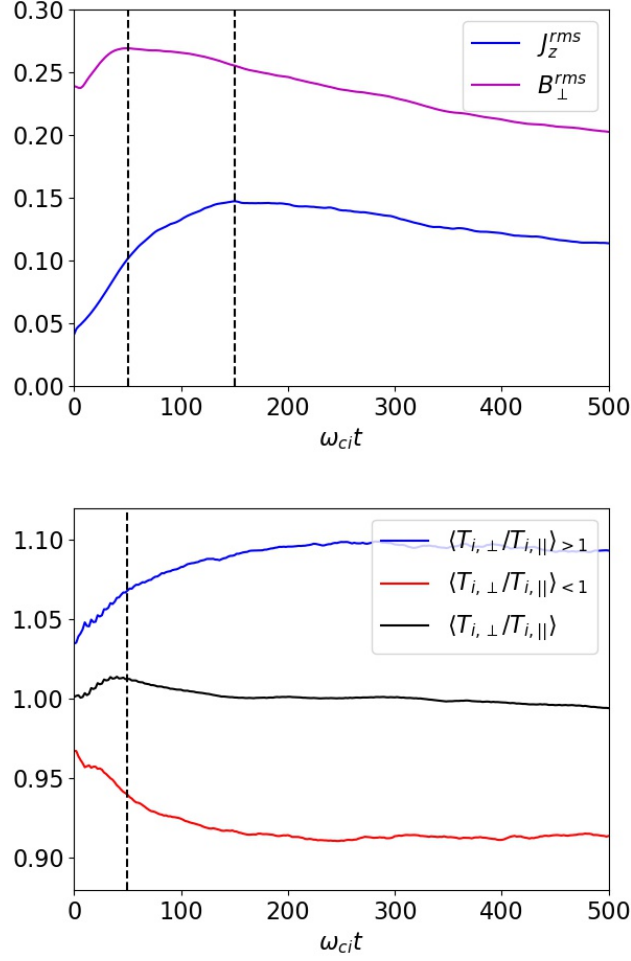


**Figure 1.** Evolution of root-mean-square values of perpendicular magnetic field  $B_{\perp}^{rms}/B_0$  and parallel current density  $J_z^{rms}/(n_0 e v_{Ai})$  (top panel). Evolution of ion temperature anisotropy  $T_{i,\perp}/T_{i,\parallel}$  averaged over the grid locations where  $T_{i,\perp}/T_{i,\parallel} > 1$  (perpendicular temperature anisotropy  $\langle T_{i,\perp}/T_{i,\parallel} \rangle > 1$ ), the locations where  $T_{i,\perp}/T_{i,\parallel} < 1$  (parallel temperature anisotropy  $\langle T_{i,\perp}/T_{i,\parallel} \rangle < 1$ ) and all the locations (net temperature anisotropy  $\langle T_{i,\perp}/T_{i,\parallel} \rangle$ ) in the simulation domain (bottom panel). Vertical dashed lines are drawn at  $\omega_{ci}t = 50$  and  $\omega_{ci}t = 150$  (only in top panel).

the central current) providing current closure. The central current has relatively sharper variation. These current sheets break up developing their own turbulence by  $\omega_{ci}t = 150$ .

Fig. 1 also shows the evolutions of various averages of the ion temperature anisotropy  $T_{i,\perp}/T_{i,\parallel}$ . Net average ion temperature anisotropy  $\langle T_{i,\perp}/T_{i,\parallel} \rangle$ , obtained by averaging  $T_{i,\perp}/T_{i,\parallel}$  over the whole simulation grid, grows to reach a peak a little before  $\omega_{ci}t = 50$  (the time by which current sheets

have formed) with a value slightly above its initial isotropic value of unity and then drops to saturate around the isotropic value. On the other hand, average perpendicular and parallel ion temperature anisotropies,  $\langle T_{i,\perp}/T_{i,\parallel} \rangle_{>1}$  and  $\langle T_{i,\perp}/T_{i,\parallel} \rangle_{<1}$  (obtained by averaging  $T_{i,\perp}/T_{i,\parallel}$  over the simulation grid locations where  $T_{i,\perp}/T_{i,\parallel} > 1$  and  $T_{i,\perp}/T_{i,\parallel} < 1$ , respectively) continue to develop beyond the peak of  $\langle T_{i,\perp}/T_{i,\parallel} \rangle$  and saturate later to the values  $\approx 1.10$  and  $0.90$  (10% anisotropy), respectively. This means that both the perpendicular and parallel temperature anisotropies exist in turbulence despite the net temperature anisotropy indicating isotropy.

Our interest in this paper is in free energy sources empowering plasma instabilities in current sheets formed in turbulence. Therefore we examine these current sheets at  $\omega_{ci}t = 50$  to look for available free energy sources well before their depletion by the growth of plasma instabilities. The time  $\omega_{ci}t = 50$  is also the time of the perpendicular magnetic energy  $\int |\mathbf{B}_\perp|^2 dx dy \propto (B_\perp^{rms})^2$  reaching maximum (Fig. 1). Current sheets store magnetic energy and therefore the time of magnetic energy reaching maximum can be taken as the time of peak activity of current sheet formation. Analysis of current sheets at other times shows that the conclusions presented in this paper are independent of the choice of the analysis time around  $\omega_{ci}t = 50$ .

Figs. 3 and 4 show various quantities at  $\omega_{ci}t = 50$  in a quarter of the simulation plane (the top-left quadrant of the planes shown in Fig. 2) to inspect the free energy sources provided by the spatial gradients of  $n$ ,  $\mathbf{u}_e$  and  $\mathbf{u}_i$  in current sheets. Fig. 5 shows the line-outs of these quantities along a randomly chosen line  $y/d_i=85$ . It is evident that parallel current density  $J_z$  in current sheets (Fig. 3a) is almost entirely contributed by parallel electron bulk velocity  $u_{ez}$  (Fig. 3c) which is much larger than the parallel ion bulk velocity  $u_{iz}$  inside current sheets (Fig. 3d). Line-outs in Fig. 5a show that  $|u_{iz}| < |u_{ez}|$  except when  $J_z$  is very small. Plasma number density has strong gradients inside current sheets in comparison to out-side current sheets but its variation (under 10% about the mean value  $n/n_0 = 1$ ) inside current sheets does not affect significantly the current sheet structure.

In our simulations,  $u_{ez}$  in current sheets is at least eight times larger than the global root-mean-square value of  $u_{iz}$ ,  $|u_{ez}|/u_{iz,rms} \gtrsim 8$  (Fig. 6a). In order to check if the condition  $|u_{ez}|/u_{iz,rms} \gtrsim 8$  in our simulations is specific to current sheets, we set to zero the values of  $J_z$  at the grid points where

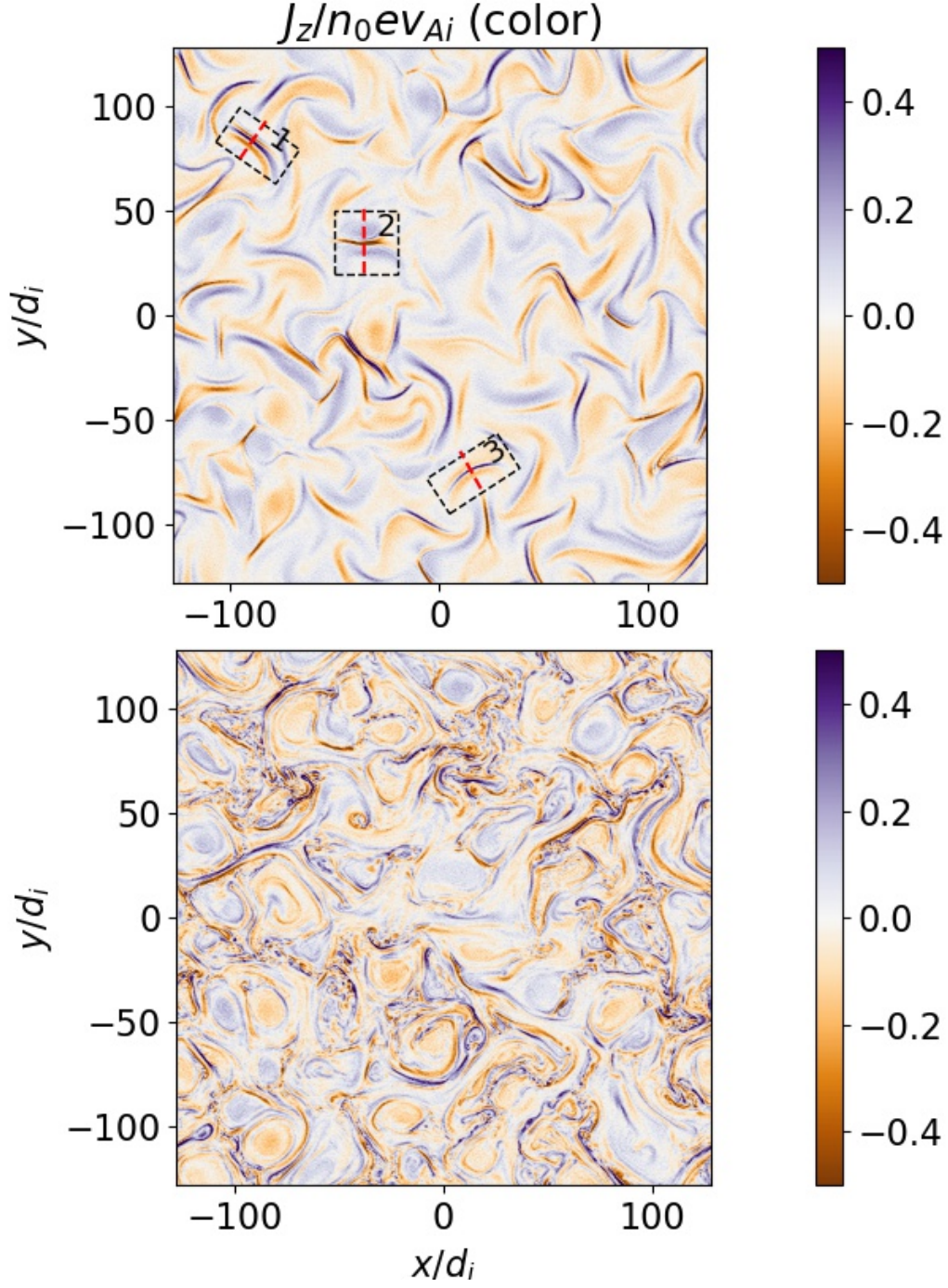


**Figure 2.** Out-of-plane current density  $J_z$  in the  $x$ - $y$  simulation plane at  $\omega_{ci}t = 50$  (top) and 150 (bottom). Three current sheets selected for detailed analysis are highlighted in the top panel by enclosing them in boxes and are numbered 1-3.

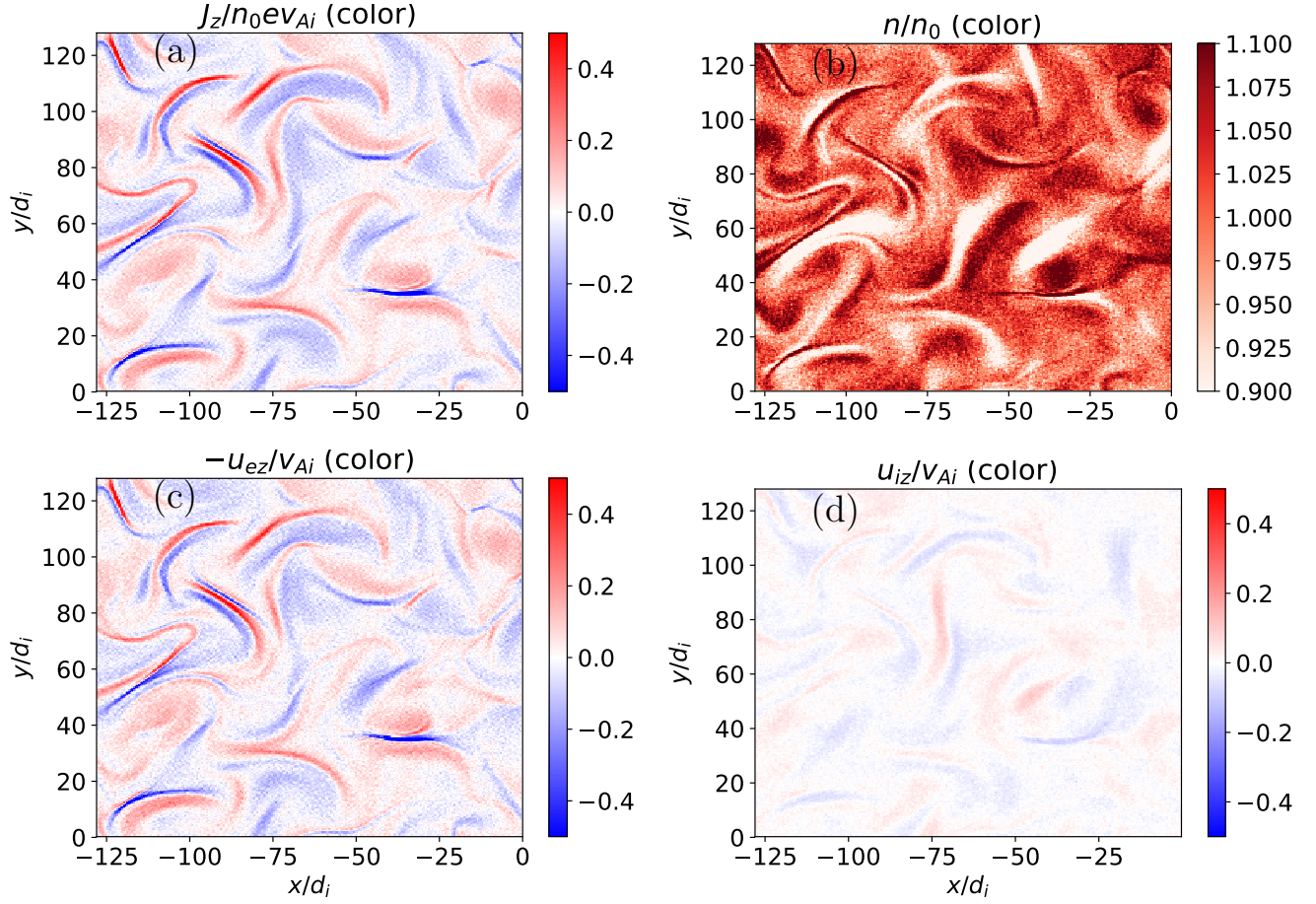


**Figure 3.** Parallel current density  $J_z$  (a), plasma number density  $n$  (b), negative of parallel electron bulk velocity  $-u_{ez}$  (c) and parallel ion bulk velocity (d) in the top-left quadrant of the simulation domain at  $\omega_{ci}t = 50$ .

the condition is not satisfied, i.e., where  $|u_{ez}|/u_{iz,rms} < 8$ . The non-zero values of the so conditioned  $J_z$ , plotted in Fig. 6b, correspond to the locations where the condition is satisfied and fall primarily in current sheets endorsing the specificity of the condition to current sheets formed in our simulations. Note that the number on the RHS of the inequality  $|u_{ez}|/u_{iz,rms} \gtrsim 8$  is not universal for collisionless plasma turbulence but is specific to the parameters of our simulations. This number, however, would always be much greater than unity as long as the current sheets thin down to below ion inertial length.

Perpendicular electron bulk velocity, shown in Fig. 4a, also develops gradients in and around current sheets. In a sharp contrast to the parallel component, its magnitude is almost equal to the

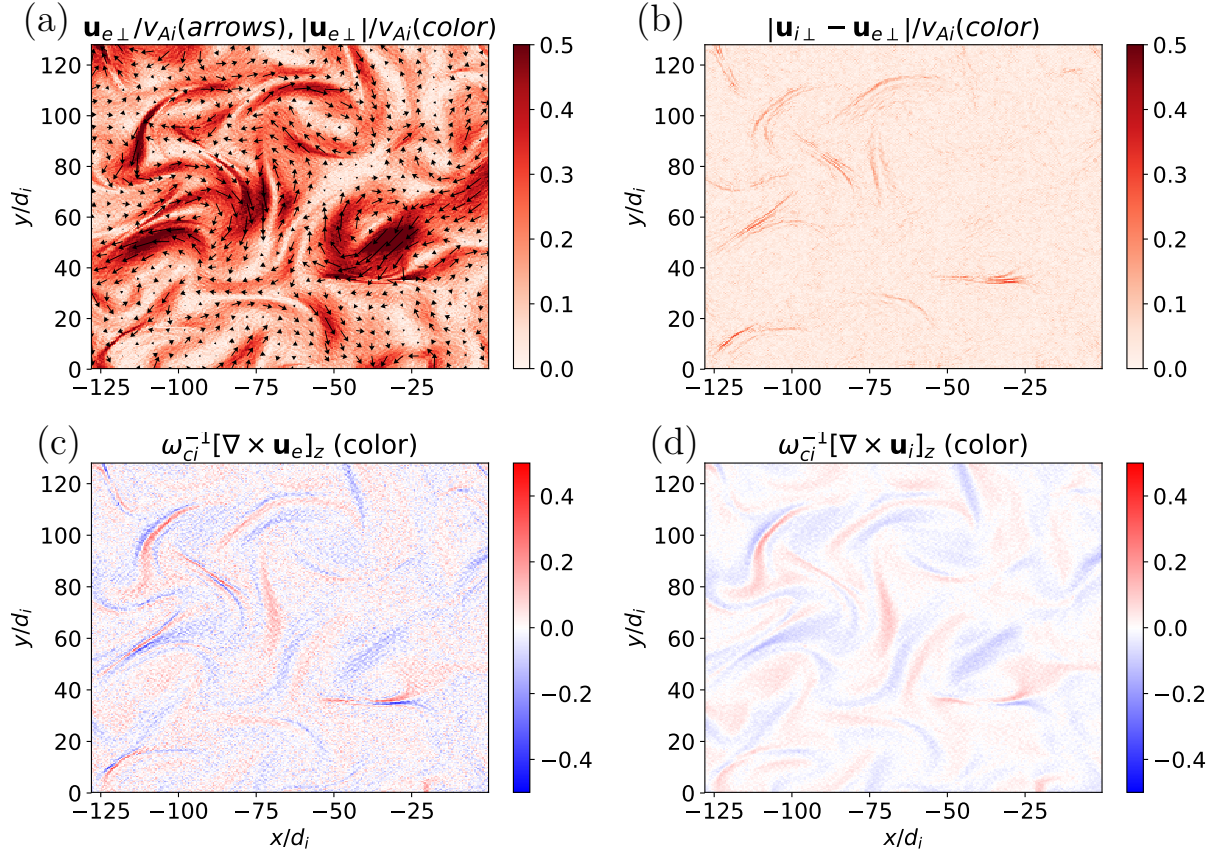


**Figure 4.** Magnitude (color) and vectors (arrows) of perpendicular electron bulk velocity (a), magnitude of the difference of perpendicular ion and electron bulk velocities (b), parallel electron (c) and ion (d) vorticities shown in the top-left quadrant of the full simulation domain at  $\omega_{ci}t = 50$ .

magnitude of the perpendicular ion bulk velocity. The difference in the two, shown in Fig. 4b, is noticeable only around current sheets. Line-outs in Fig. 5b show that significant difference in the magnitudes of the two occur where  $|\mathbf{u}_{e\perp}|$  has relatively sharper variation.

A measure of perpendicular shear flows is parallel flow vorticity which develop near current sheets for both the ion and electron flows, as shown Fig. 4c and 4d. Development of parallel ion vorticity near current sheets has been observed in other particle-in-cell (PIC) and PIC-hybrid simulations (Franci et al. 2015; Parashar & Matthaeus 2016). Our simulations, on the other hand, show development of parallel electron vorticity near current sheets. The two vorticities are of the same order of magnitude with electron vorticity typically larger than the ion vorticity (Fig. 5c).

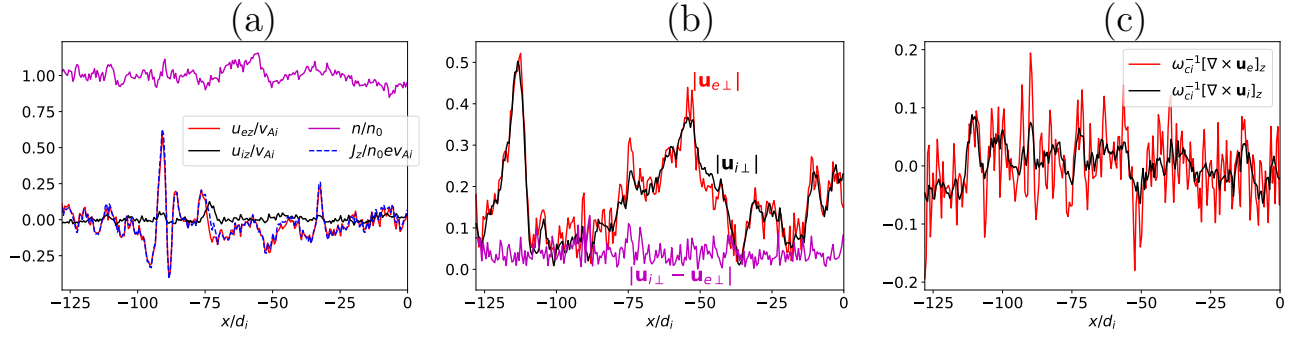


**Figure 5.** Line-outs along the line  $y/d_i \approx 85$  at  $\omega_{ci}t = 50$ . (a)  $n$ ,  $u_{ez}$ ,  $u_{iz}$  and  $J_z$ ; (b)  $|u_{e\perp}|$ ,  $|u_{i\perp}|$  and  $|u_{i\perp} - u_{e\perp}|$ ; (c)  $[\nabla \times \mathbf{u}_e]_z$  and  $[\nabla \times \mathbf{u}_i]_z$ .

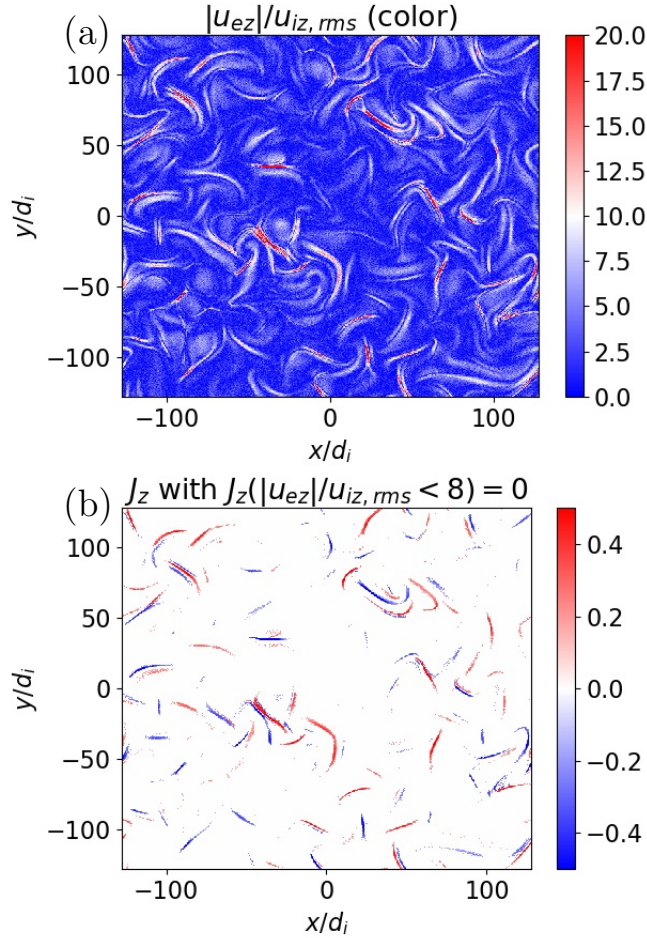


**Figure 6.** Ratio  $|u_{ez}|/u_{iz,rms}$  of magnitude of parallel electron bulk velocity  $|u_{ez}|$  and root-mean-square value of parallel ion bulk velocity  $u_{iz,rms}$  (a) and current density whose values are set to zero wherever  $|u_{ez}|/u_{iz,rms} < 8$  (b) in the full simulation domain at  $\omega_{ci}t = 50$ .

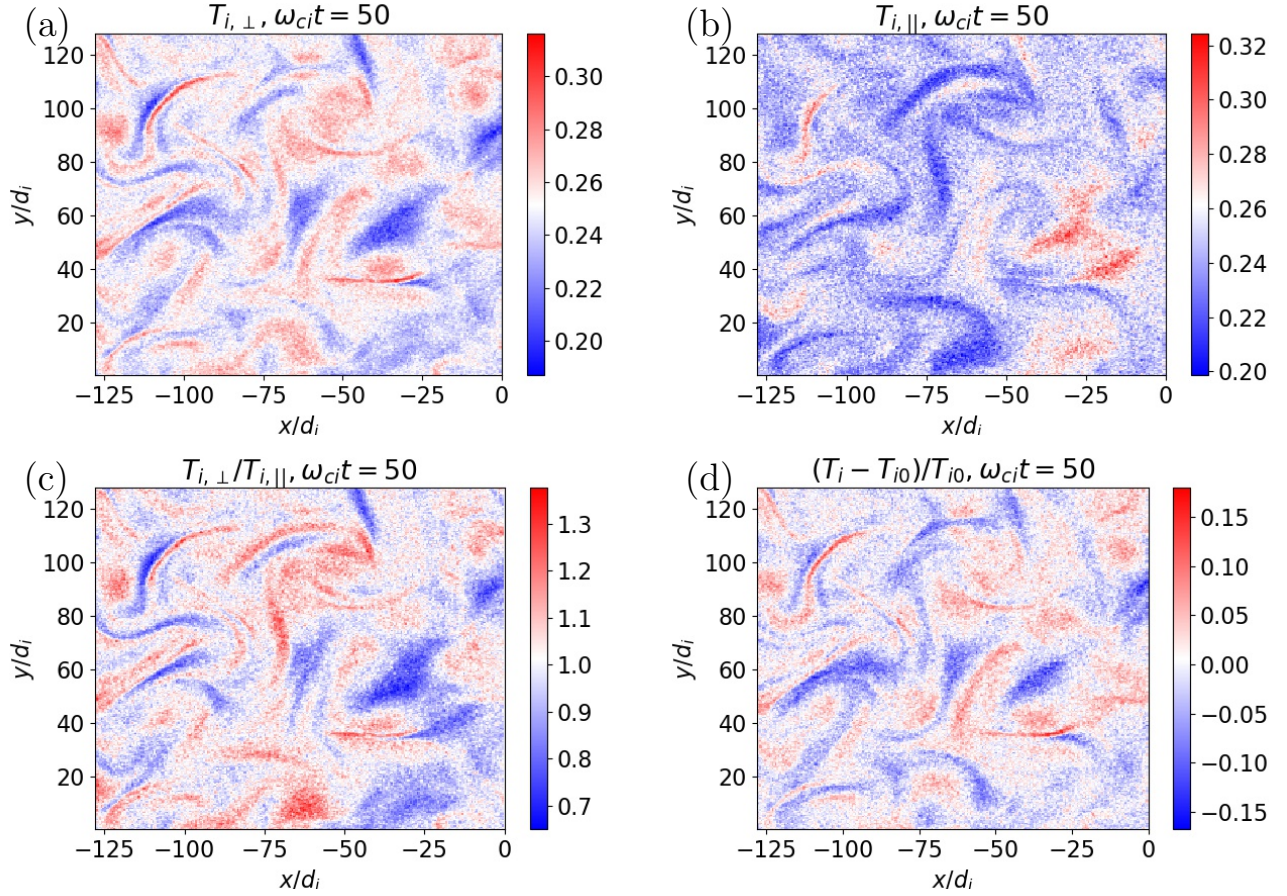


**Figure 7.** Perpendicular (a) and parallel (b) ion temperatures ( $T_{i,\perp}$  and  $T_{i,\parallel}$ ), ion temperature anisotropy  $T_{i,\perp}/T_{i,\parallel}$  (c) and fractional change  $(T_i - T_{i0})/T_{i0}$  in total ion temperature  $T_i = (2T_{i,\perp} + T_{i,\parallel})/3$  with respect to its initial value  $T_{i0}$  (d) shown in the top-left quadrant of the full simulation domain at  $\omega_{ci}t = 50$ .

By the time current sheets form, initially isotropic distribution of ions develops different temperatures parallel and perpendicular to the mean magnetic field (Fig. 7a and 7b). This results in development of both the parallel ( $T_{i,\perp}/T_{i,\parallel} < 1$ ) and perpendicular ( $T_{i,\perp}/T_{i,\parallel} > 1$ ) ion temperature anisotropy in the turbulence (Fig. 7c). Ions have also undergone both heating and cooling by  $\omega_{ci}t = 50$  (Fig. 7d). The regions of heating/cooling and perpendicular/parallel anisotropy are structured mostly around current sheets consistent with other PIC and PIC-hybrid simulations (Franci et al. 2016; Wan et al. 2015).

Fig. 8a, 8c and 8e respectively show that, ignoring few outliers, ion temperature anisotropy, change in ion temperature from its initial value, and perpendicular ion temperature are well correlated with

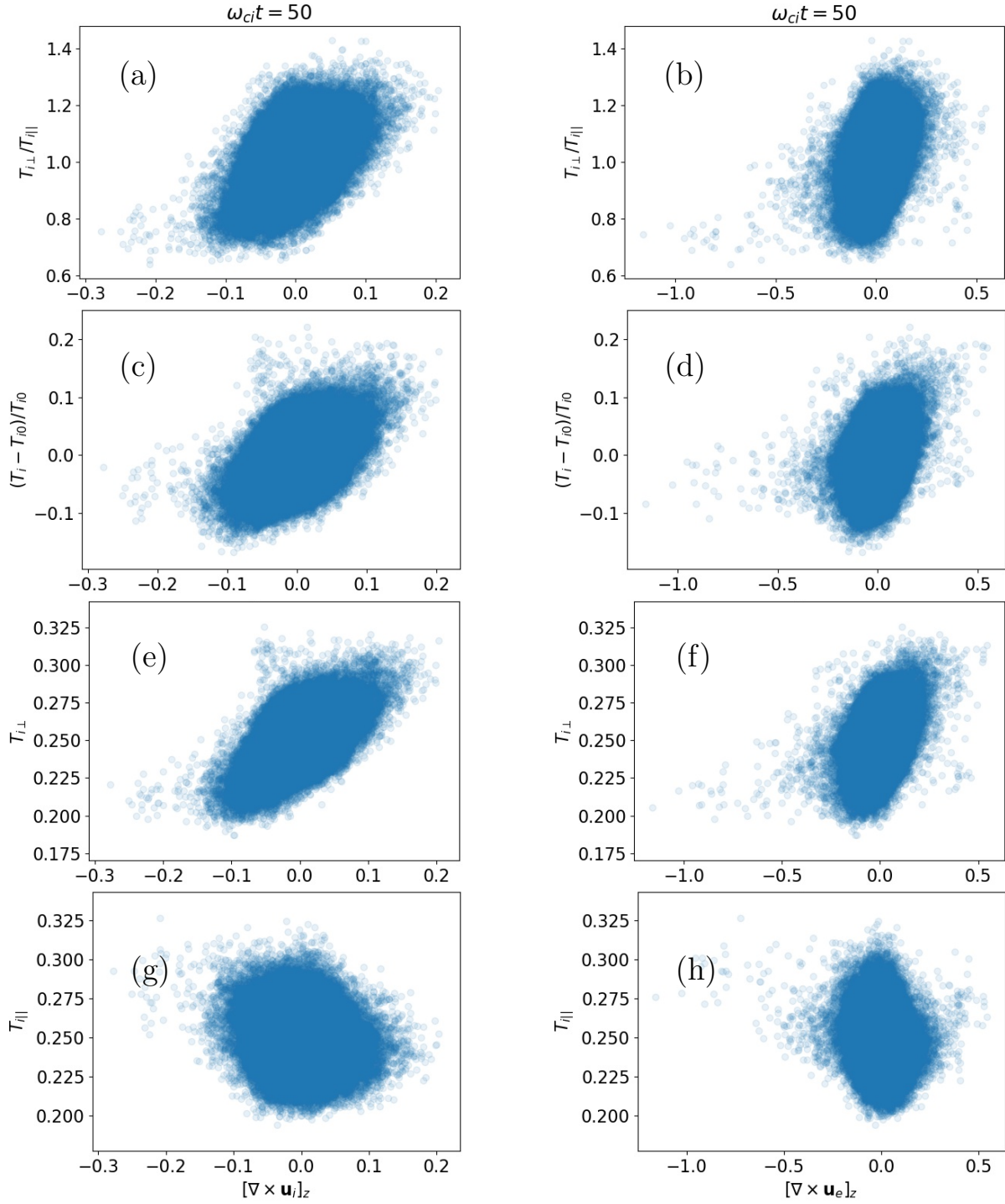


**Figure 8.** Scatter plots of ion temperature anisotropy  $T_{i,\perp}/T_{i,\parallel}$  (first row), fractional change in ion temperature  $(T_i - T_{i0})/T_{i0}$  (second row), and perpendicular (third row) and parallel (fourth row) ion temperatures ( $T_{i,\perp}$  and  $T_{i,\parallel}$ ) with parallel ion (first column) and electron (second column) vorticities at  $\omega_{ci}t = 50$ .

parallel ion flow vorticity. Parallel ion temperature, on the other hand, seems to have relatively weak anti-correlation with the parallel ion flow vorticity (Fig. 8g). These correlations/anti-correlations with the parallel ion flow vorticity have earlier been reported in PIC-hybrid simulations (Franci et al. 2016). We additionally found here that the three quantities, viz., ion temperature anisotropy, change in ion temperature from its initial value, and perpendicular ion temperature, are well correlated with parallel electron flow vorticity as well (Fig. 8b, 8d and 8f). Parallel ion temperature, however, does not have correlation/anti-correlation with the electron flow vorticity (Fig. 8h).

Note that earlier PIC-hybrid simulations reported the development of ion temperature anisotropy and its correlation with ion flow vorticity at the time of the maximum turbulent activity, which was taken to be the time when RMS value of parallel current density peaks. Our results presented here, however, show that ion temperature anisotropy exhibits similar behavior at the time when current sheets have just formed ( $\omega_{ci}t = 50$ ), much earlier than the time of maximum turbulent activity ( $\omega_{ci}t = 150$  in our simulations, see Fig. 1). It implies that the processes of current sheet formation themselves contribute to ion heating/cooling and development of ion temperature anisotropy in collisionless plasma turbulence. Additional contributions are expected to come from current sheet instabilities.

We now turn our attention to individual current sheets. We select three current sheets, numbered 1-3 in Fig. 2, from the full simulation domain based on the criteria that they are relatively isolated from neighboring current sheets so that the features of an individual current sheet are discernible. Line-outs of various electron and ion quantities along the current sheet normals are shown in Fig. 9 at  $\omega_{ci}t = 50$ . The current sheet characteristics already observed in Figs. 3 and 4 can now be appreciated in individual current sheets: return current system with dominance of parallel electron bulk velocity and relatively slow variation of plasma number density (Fig. 9a-9c), similar magnitudes of perpendicular electron and ion bulk velocities except in current sheets (Fig. 9d-9f), development of parallel ion and electron vorticities (Fig. 9g-9i).

Additional details on current sheet characteristics can also be seen in the line-outs. Magnitude of the perpendicular electron bulk velocity in current sheets is significantly smaller than the parallel electron bulk velocity. Therefore electric current in the sheets flow primarily parallel to the applied

magnetic field. Perpendicular electron bulk velocity and parallel electron vorticity in current sheets vary faster than their ion counterparts. Parallel electron vorticity is larger than parallel ion vorticity in current sheets and changes sign close to the current sheet center to have opposite peaks near the current sheet edges. Such a behavior is not very clear for the parallel ion vorticity.

With the change in sign of parallel electron vorticity across the current sheets CS2 and CS3, the deviation of the perpendicular to parallel ion temperature ratio from its isotropic value of unity,  $T_{i,\perp}/T_{i,\parallel} - 1$ , also changes sign (Fig. 9k and 9l). This is consistent with the correlation of ion temperature anisotropy with parallel electron vorticity shown in Fig. 8b, i.e., perpendicular/parallel anisotropy for positive/negative electron vorticity. Ion temperature anisotropy in the current sheet CS1, however, only partially obey the correlation — perpendicular anisotropy for positive electron vorticity but no parallel anisotropy for negative electron vorticity (Fig. 9j). Also, parallel and perpendicular anisotropy comparable to those in current sheets are also present outside the current sheets where parallel electron vorticity is small. These observations suggest that temperature anisotropy is not always associated with the parallel electron vorticity.

#### 4. THEORETICAL ESTIMATES

At the ion kinetic scales, magnetic field frozen into electron bulk velocity is pushed around in the course of turbulence dynamics. The resulting time dependence of the perpendicular magnetic field  $\mathbf{B}_\perp$  generates an inductive electric field  $E_z$  parallel to the applied magnetic field according to Faraday's law  $\nabla \times E_z \hat{z} = -\partial \mathbf{B}_\perp / \partial t$ . Ions are accelerated in the z-direction by this electric field. At the scale of current sheet thickness  $\sim d_i = \sqrt{2}\rho_i$ , ions can be approximated as un-magnetized. Then the parallel ion bulk velocity evolves as,

$$\frac{\partial u_{iz}}{\partial t} = \frac{e}{m_i} E_z, \quad (3)$$

where convective derivative  $\mathbf{u}_i \cdot \nabla u_{iz}$  has been assumed to be small. Parallel electron bulk velocity adjusts to satisfy Ampere's law and evolves as,

$$\frac{\partial u_{ez}}{\partial t} = \frac{e}{m_i} (E_z - d_i^2 \nabla^2 E_z), \quad (4)$$

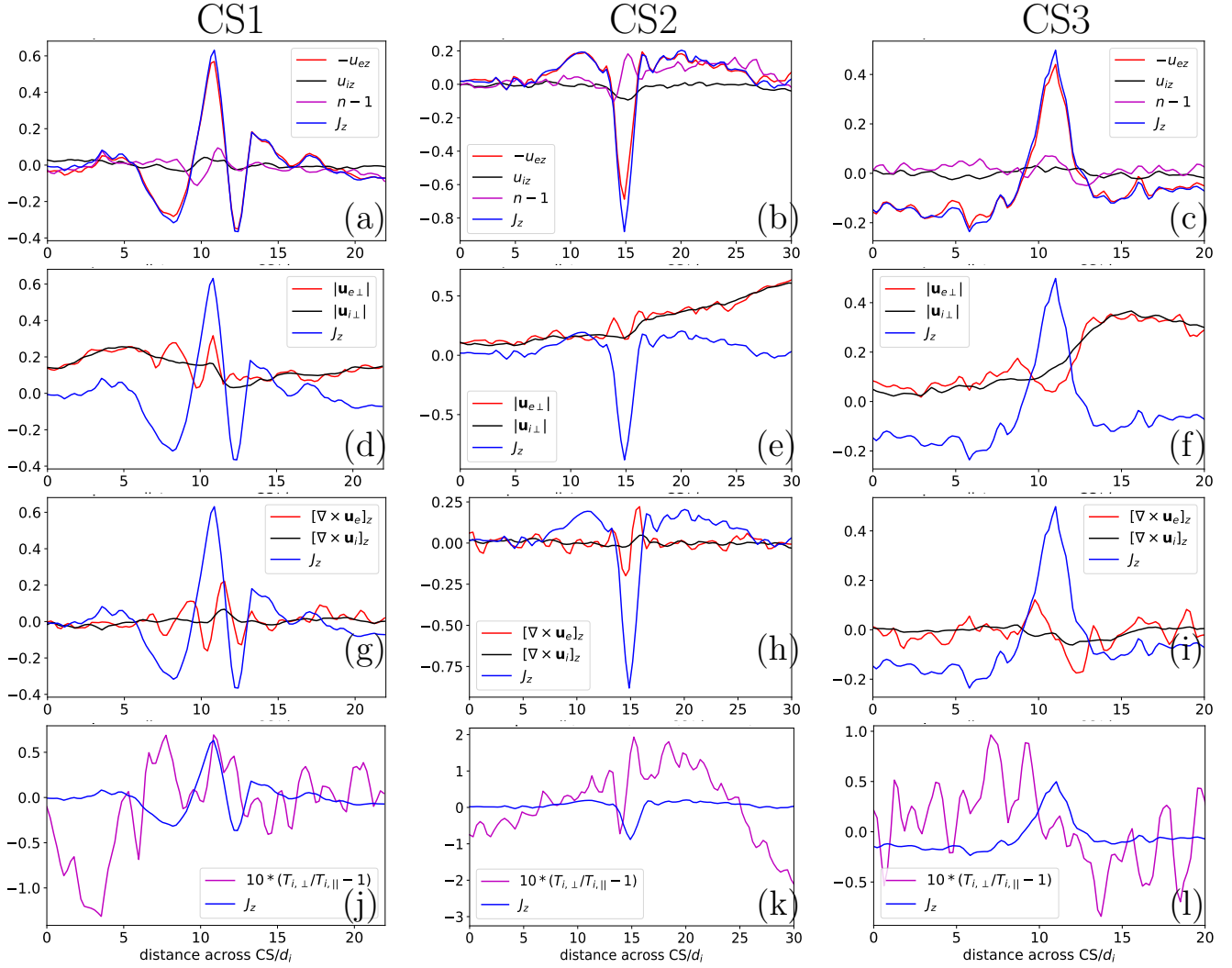


**Figure 9.** Line-outs along the current sheet normals numbered 1 (left column, CS1), 2 (middle column, CS2) and 3 (right column, CS3) in Fig. 2 at  $\omega_{ci}t = 50$ . Line-outs of  $-u_{ez}/v_{Ai}$ ,  $u_{iz}/v_{Ai}$ ,  $n/n_0 - 1$  (first row),  $|\mathbf{u}_{e\perp}|/v_{Ai}$ ,  $|\mathbf{u}_{i\perp}|/v_{Ai}$  (second row),  $\omega_{ci}^{-1}[\nabla \times \mathbf{u}_e]_z$ ,  $\omega_{ci}^{-1}[\nabla \times \mathbf{u}_i]_z$  (third row) and deviation from temperature isotropy  $10 \times (T_{i,\perp}/T_{i,\parallel} - 1)$  (fourth row). Electron and quantities are plotted by red and black lines, respectively. Line-out of  $J_z/n_0 v_{Ai}$  is plotted by blue line in all the sub-plots.

obtained by taking time derivative of Ampere's law, neglecting time derivative of plasma density, and making use of Eq. (3) and Faraday's law. Note that Eq. (4) is not the same as the electron momentum equation where the time-derivative of electron bulk velocity appears as an electron inertial term, i.e., multiplied by electron mass. In the hybrid simulation model used in this paper, the electron inertial terms in the electron momentum equation are neglected.

Estimating  $|u_{iz}| \sim |\tau e E_z / m_i|$  and  $|u_{ez}| \sim |\tau e E_z (1 - d_i^2 / L^2) / m_i|$  from Eqs. (3) and (4), respectively, and  $|E_z| \sim L |\mathbf{B}_\perp| / \tau$  from Faraday's law,

$$\frac{|u_{iz}|}{v_{Ai}} \sim \frac{L}{d_i} \frac{|\mathbf{B}_\perp|}{B_0} \quad (5)$$

and,

$$\frac{|u_{ez}|}{v_{Ai}} \sim \frac{L}{d_i} \frac{|\mathbf{B}_\perp|}{B_0} \left| 1 - \frac{d_i^2}{L^2} \right|. \quad (6)$$

Here  $L$  is the scale length of the  $E_z$ -variation (typically the same as the current sheet thickness) and  $\tau$  is the time available for the formation of current sheets before they are disrupted by either the instabilities in current sheets or the turbulence dynamics. Here, we refer to  $L$  as the current sheet thickness. The ratio of  $|u_{ez}|$  and  $|u_{iz}|$  gives,

$$\frac{|u_{ez}|}{|u_{iz}|} \sim \left| 1 - \frac{d_i^2}{L^2} \right| \quad (7)$$

In the limit  $L \ll d_i$ ,  $|u_{ez}| \propto d_i / L$  and Eq. (7) gives  $|u_{ez}| / |u_{iz}| \sim d_i^2 / L^2 \gg 1$ . The thinner the current sheet is, larger (smaller) the parallel electron (ion) bulk velocity and the current in the sheet is increasingly carried by electrons. In current sheets with sub- $d_i$  scale lengths, say  $L = 0.5 d_i$ ,  $|u_{ez}| / |u_{iz}| \sim 3$ , consistent with the simulation results. In the opposite limit  $L \gg d_i$  valid outside current sheets,  $|u_{ez}| / |u_{iz}| \rightarrow 1$ , again consistent with the simulation results.

The perpendicular electron bulk velocity is simply the  $E \times B$  drift as per Ohm's law in hybrid plasma models without electron inertia. Outside current sheets, ions are magnetized and also execute  $E \times B$  drift in the plane of simulation resulting in  $|\mathbf{u}_{e\perp}| \approx |\mathbf{u}_{i\perp}|$ . They are, however, un-magnetized inside or near current sheets and therefore their in-plane motion deviates from the in-plane electron motion. The difference between perpendicular electron and ion bulk velocities given by Ampere's law,  $|\mathbf{u}_{i\perp} - \mathbf{u}_{e\perp}| / v_{Ai} = d_i |\nabla_\perp \times B_z \hat{z}| / B_0 \sim (d_i / L) (B_z / B_0)$ , is inversely proportional to the gradient scale length resulting in  $|\mathbf{u}_{e\perp}| \neq |\mathbf{u}_{i\perp}|$  in current sheets, as can be seen from Fig. 9d-9f.

Due to the difference between the perpendicular electron and ion bulk velocities, parallel vorticity also differ in current sheets. This difference can be obtained by taking curl of Ampere's law which

gives,

$$[\nabla \times \mathbf{u}_i - \nabla \times \mathbf{u}_e]_z = -\omega_{ci} d_i^2 \nabla^2 B_z \quad (8)$$

The difference is maximum where second derivative of  $B_z$  is largest.

## 5. DISCUSSION AND CONCLUSION

We carried out two-dimensional PIC-hybrid-code simulations of a collisionless turbulent plasma ( $\beta_i = \beta_e = 0.5$ ) in an external magnetic field perpendicular to the simulations plane in a large simulation box ( $256d_i \times 256d_i$ ). We initiated the plasma turbulence by long-wavelength random-phased magnetic fluctuations. The simulations show formation of current sheets in turbulent plasma. We examined the potential sources of free energy available for an unstable decay of these current sheets: spatial gradients of the plasma density and electron/ion bulk velocities. By simulations and analytical estimates we could show that the magnetic-field-aligned (parallel) electron bulk velocity  $u_{ez} \gg |\mathbf{u}_{e\perp}| \sim |\mathbf{u}_{i\perp}|$  and  $u_{ez} \gg u_{iz}$  dominates the current density  $\mathbf{J} = ne(\mathbf{u}_{i\perp} + u_{iz}\hat{z} - \mathbf{u}_{e\perp} - u_{ez}\hat{z})$  in the sheets, i.e. the sheet currents flows primarily parallel to the external magnetic field. The electron bulk velocity component in the direction perpendicular to the magnetic field ( $\mathbf{u}_{e\perp}$ ), though of the same order of magnitude as the perpendicular ion bulk velocity ( $\mathbf{u}_{i\perp}$ ), varies faster than  $\mathbf{u}_{i\perp}$  through the current sheets. As a consequence the parallel electron vorticity exceeds and varies faster through the current sheets than parallel ion vorticity. At the same time the variation of the plasma number density through the current sheets is small. Therefore, we conclude, the primary source of free energy for instabilities of current sheets formed in collisionless plasma turbulence is the electron shear flow in the directions parallel and perpendicular to the external magnetic field.

We found that the (half-)thickness of the current sheets formed in the turbulent plasma were at most ion inertial lengths  $d_i$  in simulations with a spatial resolution of  $0.5d_i$ . Simulations with increased grid resolution have shown that current sheets always thin down to the scale of the grid resolution while the peak value of the magnetic-field aligned (parallel) current density increases in agreement with Eq. (7). This means that the current sheet thickness in our simulations was controlled by numerical effects at grid scales. Hence, in a collisionless plasma current sheets continue to thin down

until a physical effect stops the thinning. In collisionless plasmas this will be, finally, the electron inertia. The thickness of current sheets formed in collisionless plasma turbulence, therefore, cannot be determined by just continuing to decrease grid spacing in hybrid simulations without taking into account electron inertia. Instead it is necessary to include the electron inertia in the fluid description of electrons in the framework of hybrid codes to determine the current sheet thickness.

Note that in laboratory reconnection experiments with strong external (guide-) magnetic fields like the Greifswald VINETA.II experiment sheets of electron dominated current flows parallel to the external magnetic field and electron shear flows in the perpendicular direction were found (von Stechow et al. 2016). Hence, the formation of such thin current sheets seems to be generic in collisionless plasmas with external magnetic field. Electron-magnetohydrodynamic simulations carried out to understand the results of the laboratory experiments revealed that plasma instabilities driven by perpendicular electron shear flows generate magnetic fluctuation as they were found in the experiments, if the electron inertia is taken into account (Jain et al. 2017).

## ACKNOWLEDGMENTS

We gratefully acknowledge the developers of the A.I.K.E.F. code and the financial support by the German Science Foundation (DFG), project JA 2680-2-1.

Part of the simulations were carried out on the HPC-Cluster of the Institute for Mathematics at the TU Berlin and the Max-Planck-Institute for Solar System Research Göttingen. .

## REFERENCES

- |   |  |
|---|--|
| <p>Bale, S. D., Kellogg, P. J., Mozer, F. S., Horbury, T. S., &amp; Reme, H. 2005, Physical Review Letters, 94, 215002, doi: <a href="https://doi.org/10.1103/PhysRevLett.94.215002">10.1103/PhysRevLett.94.215002</a></p> <p>Biskamp, D., &amp; Welter, H. 1989, Phys. Fluids B, 1, 1964</p> | <p>Borovsky, J. E. 2010, Phys. Rev. Lett., 105, 111102, doi: <a href="https://doi.org/10.1103/PhysRevLett.105.111102">10.1103/PhysRevLett.105.111102</a></p> <p>Borovsky, J. E., &amp; Podesta, J. J. 2015, J. Geophys. Res.: Space Phys., 120, 9256</p> <p>Bourouaine, S., &amp; Chandran, B. D. G. 2013, Astrophys. J., 774, 96, <a href="http://stacks.iop.org/0004-637X/774/i=2/a=96">http://stacks.iop.org/0004-637X/774/i=2/a=96</a></p> |
|---|--|

- Chandran, B. D. G., Li, B., Rogers, B. N., Quataert, E., & Germaschewski, K. 2010, *Astrophys. J.*, 720, 503. <http://stacks.iop.org/0004-637X/720/i=1/a=503>
- Chasapis, A., Matthaeus, W. H., Parashar, T. N., et al. 2017, *Astrophys. J.*, 836, 247. <http://stacks.iop.org/0004-637X/836/i=2/a=247>
- Demchenko, V. V., & Hussein, A. M. 1974, *Nucl. Fusion*, 14, 229. <http://stacks.iop.org/0029-5515/14/i=2/a=008>
- Dmitruk, P., Matthaeus, W. H., & Seenu, N. 2004, *Astrophys. J.*, 617, 667
- Drake, J. F., Swisdak, M., Che, H., & Shay, M. A. 2006, *Nature*, 443, 553
- Egedal, J., Daughton, W., & Le, A. 2012, *Nature Physics*, 8, 321
- Ergun, R., Chen, L.-J., Wilder, F., et al. 2017, *Geophysical Research Abstracts*, 19, EGU2017. <http://meetingorganizer.copernicus.org/EGU2017/EGU2017-8740-1.pdf>
- Franci, L., Landi, S., Matteini, L., Verdini, A., & Hellinger, P. 2015, *Astrophys. J.*, 812, 21, doi: 10.1088/0004-637X/812/1/21
- . 2016, *Astrophys. J.*, 833, 91. <http://stacks.iop.org/0004-637X/833/i=1/a=91>
- Gary, S. P., Hughes, R. S., & Wang, J. 2016, *Astrophys. J.*, 816, 102
- Gingell, P. W., Burgess, D., & Matteini, L. 2015, *Astrophys. J.*, 802, 4
- Hollweg, J. V., & Isenberg, P. A. 2002, *J. Geophys. Res.: Space Physics*, 107, SSH 12, doi: 10.1029/2001JA000270
- Howes, G. G. 2015, *Phil. Trans. R. Soc. A*, 373, 20140145, doi: 10.1098/rsta.2014.0145
- . 2016, *Astrophys. J. Lett.*, 827, L28. <http://stacks.iop.org/2041-8205/827/i=2/a=L28>
- Howes, G. G., TenBarge, J. M., Dorland, W., et al. 2011, *Phys. Rev. Lett.*, 107, 035004, doi: 10.1103/PhysRevLett.107.035004
- Jain, N., Stechow, A., Muñoz, P., et al. 2017, *Phys. Plasmas*, 24, 092312
- Karimabadi, H., Roytershteyn, V., Wan, M., et al. 2013, *Phys. Plasmas*, 20, 012303, doi: <http://dx.doi.org/10.1063/1.4773205>
- Leamon, R. J., Matthaeus, W. H., Smith, C. W., & Wong, H. K. 1998, *Astrophys. J. Lett.*, 507, L181
- Loureiro, N. F., & Boldyrev, S. 2017, *Phys. Rev. Lett.*, 118, 245101, doi: 10.1103/PhysRevLett.118.245101
- Markovskii, S. A., & Vasquez, B. J. 2011, *Astrophys. J.*, 739, 22. <http://stacks.iop.org/0004-637X/739/i=1/a=22>
- Markovskii, S. A., Vasquez, B. J., & Smith, C. W. 2008, *Astrophys. J.*, 675, 1576. <http://stacks.iop.org/0004-637X/675/i=2/a=1576>
- Maron, J., & Goldreich, P. 2001, *Astrophys. J.*, 554, 1175. <http://stacks.iop.org/0004-637X/554/i=2/a=1175>
- Marsch, E. 2006, *Living Rev. Solar Phys.*, 3, 1, doi: 10.1007/lrsp-2006-1
- Matthaeus, W. H., Wan, M., Servidio, S., et al. 2015, *Phil. Trans. R. Soc. A*, 373, 20140154, doi: 10.1098/rsta.2014.0154

- Müller, J., Simon, S., Motschmann, U., et al. 2011, *Comput. Phys. Commun.*, 182, 946, doi: <http://dx.doi.org/10.1016/j.cpc.2010.12.033>
- Muñoz, P. A., & Büchner, J. 2017, arXiv:1705.01066 [physics.plasm-ph]
- Osman, K. T., Matthaeus, W. H., Gosling, J. T., et al. 2014, *Phys. Rev. Lett.*, 112, 215002, doi: [10.1103/PhysRevLett.112.215002](https://doi.org/10.1103/PhysRevLett.112.215002)
- Osman, K. T., Matthaeus, W. H., Greco, A., & Servidio, S. 2011, *Astrophys. J. Lett.*, 727, L11. <http://stacks.iop.org/2041-8205/727/i=1/a=L11>
- Parashar, T. N., & Matthaeus, W. H. 2016, *Astrophys. J.*, 832, 57. <http://stacks.iop.org/0004-637X/832/i=1/a=57>
- Perri, S., Goldstein, M. L., Dorelli, J. C., & Sahraoui, F. 2012, *Phys. Rev. Lett.*, 109, 191101, doi: [10.1103/PhysRevLett.109.191101](https://doi.org/10.1103/PhysRevLett.109.191101)
- Podesta, J. J. 2012, *J. Geophys. Res.: Space Phys.*, 117, A07101, doi: [10.1029/2012JA017770](https://doi.org/10.1029/2012JA017770)
- . 2017, *J. Geophys. Res.: Space Phys.*, 122, 2795, doi: [10.1002/2016JA023629](https://doi.org/10.1002/2016JA023629)
- Schekochihin, A. A., Cowley, S. C., Dorland, W., et al. 2009, *Astrophys. J. Suppl.*, 182, 310, doi: [10.1088/0067-0049/182/1/310](https://doi.org/10.1088/0067-0049/182/1/310)
- Sundkvist, D., Retinò, A., Vaivads, A., & Bale, S. D. 2007, *Phys. Rev. Lett.*, 99, 025004, doi: [10.1103/PhysRevLett.99.025004](https://doi.org/10.1103/PhysRevLett.99.025004)
- TenBarge, J. M., & Howes, G. G. 2013, *Astrophys. J. Lett.*, 771, L27. <http://stacks.iop.org/2041-8205/771/i=2/a=L27>
- von Stechow, A., Grulke, O., & Klinger, T. 2016, *Plasma Phys. and Control. Fusion*, 58, 014016. <http://stacks.iop.org/0741-3335/58/i=1/a=014016>
- Wan, M., Matthaeus, W. H., Roytershteyn, V., et al. 2015, *Phys. Rev. Lett.*, 114, 175002, doi: [10.1103/PhysRevLett.114.175002](https://doi.org/10.1103/PhysRevLett.114.175002)